

# Enhancing Power Systems Transmission Adequacy via Optimal BESS Siting and Sizing using Benders Decomposition with Feasibility Cuts

Ginevra Larroux, Matthieu Jacobs, Keyu Jia, Fabrizio Sossan *Member, IEEE*, Mario Paolone, *Fellow, IEEE*

**Abstract**—This work presents a general framework for the operationally driven optimal siting and sizing of battery energy storage systems in power transmission networks, aimed at enhancing their resource adequacy. The approach considers multi-period planning horizons, enforces network constraints at high temporal resolution, and targets large-scale meshed systems. The resulting computationally complex mixed-integer non-linear programming problem is reformulated as a mixed-integer second-order cone programming problem and solved via Generalized Benders Decomposition, with feasibility cuts enabling congestion management and voltage regulation under binding network limits. A tailored heuristic recovers an alternating-current power-flow-feasible operating point from the relaxed solution. The proposed formulation is parallelizable, yielding excellent computational performance, while featuring rigorous guarantees of convergence.

**Index Terms**—Power Systems Planning, Battery Energy Storage Systems, Generalized Benders Decomposition, Mixed Integer Programming, Second-Order Cone Programming

## NOMENCLATURE

### Parameters

$\gamma/\tau$	Annualization factor, adjusted to the horizon length.
$C_s^{\min}$	Minimum, maximum installed energy limits BESS $s$ .
$C_s^{\max}$	
$C_{\text{rate}}$	Battery power C-rate.
$IC_s^e$	Investment cost per unit installed energy of BESS $s$ .
$IC_s^p$	Investment cost per unit rated power of BESS $s$ .
$OC_l$	Penalty cost associated to branch $l$ system losses.
$t^i, t^f$	Initial $i$ and final $f$ time steps of each subproblem.
$W_s^{\min}$	Minimum, maximum rated power limits of BESS $s$ .
$W_s^{\max}$	
$w_{\text{loss}}$	Weight for the cost of system losses.
$w_{\text{slack}}$	Weight for the cost of slack variables.
$SoE_s^{\min}$	Minimum, maximum state of energy of BESS $s$ .
$SoE_s^{\max}$	

### Sets

$\Lambda$	Constraints involving variables in $\Omega_2$ .
$\mathcal{B}$	Completed Benders iterations.
$\mathcal{D}$	Set of subproblems $d$ .
$\mathcal{G}$	Power generators.
$\mathcal{L}$	Network branches.
$\mathcal{N}$	Network buses.
$\mathcal{S}$	BESSs.
$\mathcal{T}$	Time steps of the planning horizon.
$\Omega_1$	Master problem variables.
$\Omega_2$	Subproblems variables.
$\Phi$	Feasible subproblems across Benders iterations.
$\Pi$	Constraints involving variables in $\Omega_1$ .
$\Xi$	Coupling constraints involving variables in $\Omega_1$ and $\Omega_2$ .

### Variables

$\alpha_d$	Proxy for the operational cost of subproblem $d$ .
$\Gamma_d^{(\beta)}$	LHS of optimality cuts.
$\theta_{n,t}$	Voltage phase at node $n$ , time $t$ .
$\Upsilon_d^{(\beta)}$	LHS of feasibility cuts.
$C_s, W_s$	Size (energy and power) variables of BESS $s$ .
$E_{s,t}$	State of energy of BESS $s$ at node $n$ , time $t$ .
$K_{ol,t}$	Equivalent ampacity constraint for power losses of branch $l$ .
$p_{n,t}$	Active power at node $n$ , time $t$ .
$P_{ng,t}$	Active power of generator $g$ at node $n$ , time $t$ .
$P_{ns,t}$	Active power of BESS $s$ at node $n$ , time $t$ .
$p_{ol,t}$	Active power losses of branch $l$ , time $t$ .
$p_{sl,t}$	Active power at sending end $s$ of branch $l$ , time $t$ .
$q_{n,t}$	Reactive power at node $n$ , time $t$ .
$Q_{ng,t}$	Reactive power of generator $g$ at node $n$ , time $t$ .
$Q_{ns,t}$	Reactive power of BESS $s$ at node $n$ , time $t$ .
$q_{ol,t}$	Reactive power losses of branch $l$ , time $t$ .
$q_{sl,t}$	Reactive power at sending end $s$ of branch $l$ , time $t$ .
$s_{C_s,t}$	Slack variable for installed energy of BESS $s$ .
$s_{W_s,t}$	Slack variable for rated power of BESS $s$ .
$U_s$	Site variables of BESS $s$ .
$V_{n,t}$	Voltage magnitude at node $n$ , time $t$ .
CAPEX	Capital expenditure.
OPEX $_d$	Operational expenditure for subproblem $d$ .

## I. INTRODUCTION

Modern power systems with high shares of stochastic generation, increasingly strain system adequacy. The strategic deployment of market-neutral battery energy storage systems (BESSs) by transmission system operators (TSOs) can improve the cost-effectiveness of re-dispatch, and reduce the need for grid reinforcement, thereby supporting the economic, safe and reliable system operation. TSOs therefore increasingly equip themselves with high-granularity market simulations that produce future net-injection trajectories and associated scenario sets. High temporal resolution is required to capture rapid intra-day fluctuations driven by intermittent and weakly dispatchable distributed energy resources (DERs), while scenario diversity captures their uncertainty. Seasonal variability in generation and demand is typically accounted for by considering annual or multi-year horizons.

In this context, this work proposes a general framework for the optimal siting and sizing of BESSs in country-scale meshed transmission networks, trading off BESSs investment costs against network operational costs (e.g., for losses). Consistent with a TSO-driven operational support perspective, network constraints (i.e., the nonlinear power flow (PF) equations) are enforced at hourly resolution over a one-year

The authors are with the École Polytechnique Fédérale de Lausanne (EPFL) and the HES-SO Valais, Switzerland, email: ginevra.larroux@epfl.ch. This work was sponsored by a consortium of industry partners (including Swissgrid) and by Innosuisse, within the “STORE” flagship project.

horizon, and boundary conditions explicitly include ampacity- and voltage-limit violations. BESSs market neutrality in day-ahead and balancing markets is imposed via hard constraints. The resulting formulation includes integer siting decisions, yielding a mixed-integer non-linear programming (MINLP) that is acknowledged to be computationally intractable for real-world system sizes.

To achieve computational tractability, this work explores potential for parallelization of the problem solution, examines optimization problem decomposition techniques and grid constraints convexification strategies, with emphasis on achieving mathematically rigorous convergence guarantees and ensuring that the adopted relaxations admit tight solutions.

A primary objective is to ensure that the method can converge to an alternating current (AC)-PF-feasible operating point. Guarantees of global optimality are desirable but secondary. Finally, for the framework to address congestion management and voltage regulation, the decomposition scheme must explicitly handle operational infeasibilities.

## II. LITERATURE REVIEW

In line with the above discussed objectives, the literature review focuses on two methodological challenges: (i) accurate modeling of the nonlinear AC-optimal power flow (OPF) equations for transmission-level applications, and (ii) ensuring computational tractability and scalability for large-scale optimization problems.

### A. Grid constraints in the optimal power flow problem

The literature adopts a broad spectrum of grid OPF models, ranging from non-approximated and non-convex AC-OPF formulations, e.g. [1], [2] (typically solved via heuristics or gradient-based schemes) to simplified representations such as direct current (DC)-OPF approximations, e.g. [3], [4], and linearized AC-OPF models, e.g. [5], [6], or convex relaxations, in particular second-order cone (SOC)- and semi-definite programming (SDP)-OPF formulations, e.g., [7]–[9]. For applications where physical feasibility and operational reliability are required, numerically robust methods (i.e., methods that reliably converge to a stable, accurate solution under finite-precision arithmetic and small perturbations in inputs, even for ill-conditioned problems [10]) and practical runtimes are essential. Under these criteria, SOC relaxations are well suited: they are tight for distribution (radial) systems, often sufficiently accurate for transmission (meshed) networks, and can be solved efficiently using commercial quadratic conic programming (QCP) solvers [11], [12] based on interior-point methods [13].

A number of studies apply second-order cone programming (SOCP) to storage systems allocation, especially in distribution systems. Works such as [7] aim to achieve dispatchability in active distribution networks (ADNs), incorporate line reinforcement as an alternative to BESSs deployment, and use Benders decomposition to improve scalability, while [8] targets energy balance and grid support in ADNs. However, extending these approaches to transmission grids is nontrivial because meshed topologies impose cycle constraints on voltage angles that can compromise relaxation tightness [14]. In addition,

they omit transmission-relevant flexibility devices such as phase shifting transformers (PSTs) and on-load tap changers (OLTCs) for voltage regulation.

*On the tightness of the second-order-cone relaxation of the optimal power flow for meshed networks:* Standard formulations of the SOC relaxation of the AC-OPF [14] do not include bus voltage and branch current angles as problem variables, and they are only reconstructed *a posteriori*, if possible. For meshed networks, however, explicit modeling of bus voltage angles is essential, as they must satisfy the cyclic conditions imposed by closed loops in the network. In [15], bus voltage angles are modeled explicitly, and several properties of the relaxation are established, with emphasis on conditions that promote or guarantee tightness of the resulting operating point. However, the authors argue that these results hold only for *radial* networks and do not extend to *meshed* transmission grids. See Section III for more details.

*On the tightness of the second-order-cone relaxation of the optimal power flow for meshed networks:* Standard formulations of the SOC relaxation of the AC-OPF [14] do not include bus voltage and branch current angles as variables; they are only reconstructed *a posteriori*, when possible. In meshed networks, however, voltage angles must satisfy cycle constraints induced by network loops. In [15], voltage angles are modeled explicitly and several properties are established, with emphasis on conditions that promote or guarantee tightness of the resulting operating point. The authors of this work argue that these results apply only to *radial* networks and do not extend to *meshed* transmission grids. Further discussion is provided in Section III. This limitation does not affect the proposed framework, but it is relevant for TSO-oriented applications where AC-feasible operating points are required.

Only a limited number of works address transmission networks. For instance, [16] considers generation and storage systems co-planning under a linearized AC-OPF, while [4] adopts a DC-OPF formulation. In both cases transmission constraints are approximated. Other contributions consider operational objectives but do not explicitly account for problem infeasibilities. For example, [17] focuses primarily on power-quality aspects, and the bi-level SOC-OPF framework in [9] optimizes BESSs allocation at the distribution level and evaluates transmission-level impacts via a duality-based method (without enforcing transmission-network constraints). Consequently, they cannot directly resolve OPF infeasibilities at the transmission level, e.g. ampacity and voltage limit violations.

### B. Optimization problem decomposition

Generalized Benders Decomposition (GBD) is the dominant approach for decomposing optimal assets siting and sizing problems [16], [18], [19]. Alternative decomposition methods for large-scale problems or hierarchical optimization include Dantzig-Wolfe (DW) decomposition, alternating direction method of multipliers (ADMM), and relaxation/cutting-hyperplane methods [20], but they are less explored for operationally driven infrastructure-planning applications. Since DW targets complicating constraints rather than complicating variables, it is particularly suitable for problems that

decompose across multiple peer substructures (as opposed to a main–subproblem hierarchy), such as multi-area optimal reactive power planning [21] or optimal BESS operation [22]. Similarly, the ADMM is widely used for decentralized OPF studies in large multi-energy or multi-area networks [23], [24].

*On the convergence of Generalized Benders Decomposition for mixed-integer second-order-cone programming problems:* Results from [25], [26], and [27] establish the standing assumptions for the convergence of the GBD algorithm. In particular, with respect to the problem formulation, convergence is guaranteed when either the master problem feasible set is finite (i.a), or a subset of the feasible region of the linking variables in all subproblems (i.b); or the set of cuts generated from the subproblem duals is finite (ii). For the application under study, condition (i.b) cannot be satisfied because the framework must explicitly handle infeasibility, i.e. violations of branch ampacity and nodal voltage limits. Conditions (i.a) and (ii) require that, respectively, the main problem variables take values from a finite discrete set, or the subproblems be linear, yielding a polyhedral dual feasible set. Furthermore, convergence of the algorithm requires that optimality and feasibility cuts be derived in accordance with Farkas’ lemma [26]. The work in [28] illustrates their formulation for problems involving convex conic constraints in Banach spaces.

*Paper contributions:* This paper develops a computationally tractable formulation for high-temporal-resolution, long-horizon operationally driven planning problems. In view of the above, the proposed paper distinguishes itself from existing literature through the following contributions:

- 1) a GBD solution scheme with rigorous convergence guarantees for both optimality and feasibility cuts in the presence of mixed-integer main variables (hence a non-finite main feasible region), enabling siting and sizing under infeasible boundary conditions;
- 2) a tailored heuristic to recover a tight solution, i.e., an AC-feasible operating point, from the SOC relaxation of the AC-OPF in *meshed* transmission networks;
- 3) high computational performance (e.g., relative to [7]), achieved through the parallelization of the subproblem solution.

### III. PROPOSED METHOD

In line with established approaches in the literature, the grid constraints in the optimal BESSs allocation problem (originally a MINLP) are relaxed, yielding a mixed-integer second-order cone programming (MISOCP) that can be efficiently decomposed using Benders decomposition.

#### A. Optimization problem decomposition with Generalized Benders Decomposition

For completeness and to introduce the notation used throughout, we briefly outline the application of Benders decomposition to the considered problem. The Benders technique decomposes the MISOCP into two stages: a main problem and a family of subproblems. Decision variables include the BESSs site (location) and size (installed energy and rated power), time-invariant variables, together with the time-variant synchronous generators’ reactive power setpoints. Other variables

include grid state and control variables, notably the active and reactive power and state of energy of BESSs.

The BESSs size variables enter both the investment decisions and the operational grid constraints; therefore serve as the linking variables in the decomposed formulation.

The main problem, formulated as a mixed-integer linear programming (MILP), selects the site and size of BESSs by minimizing their capital expenditures and a proxy of operational costs aggregated from the subproblems. Each subproblem models one day of grid operation<sup>1</sup>, formulated as a SOC-OPF and minimizes system reactive power losses<sup>2</sup> conditional on the main decisions. At each iteration, the main proposes updated linking-variable values; the subproblems assess feasibility and optimality and return the corresponding Benders cuts. This iterative exchange continues until the lower and upper bounds from the main and subproblem stages coincide within a prescribed tolerance, at which point a solution consistent with the centralized problem has been obtained. The resulting GBD scheme is outlined in Algorithm 1.

1) *Mathematical formulation:* The original non-decomposed problem, is formulated as follows

$$\begin{aligned} \min_{\Omega_1, \Omega_2} \quad & \frac{\gamma}{\tau} \cdot \text{CAPEX} + \sum_{d \in \mathcal{D}} \text{OPEX}_d \\ \text{s.t.} \quad & \Pi(\Omega_1) \leq 0 \\ & \Lambda(\Omega_2) \leq 0 \\ & \Xi(\Omega_1, \Omega_2) \leq 0 \end{aligned} \quad (1)$$

$$\text{CAPEX} = \sum_{s \in \mathcal{S}} (IC_s^p \cdot W_s + IC_s^e \cdot C_s) \quad (2a)$$

$$\text{OPEX}_d = \sum_{t \in \mathcal{T}} \left( w_{\text{loss}} \cdot \sum_{l \in \mathcal{L}} OC_l \cdot q_{ol,t}^2 \right) \quad (2b)$$

The sets  $\Omega_1 = \{U_s, W_s, C_s\}$  and  $\Omega_2 = \{V_{n,t}, \theta_{n,t}, p_{n,t}, q_{n,t}, \theta_{l,t}, p_{sl,t}, q_{sl,t}, p_{ol,t}, q_{ol,t}, K_{ol,t}, P_{ng,t}, Q_{ng,t}, P_{ns,t}, Q_{ns,t}, E_{s,t}\}$  include the main problem and the subproblems variables, respectively. The set  $\Pi(\Omega_1)$  includes the site and size constraints for BESSs<sup>3</sup>,

$$W_s \in [W_s^{\min}, W_s^{\max}] \cdot U_s \quad (3a)$$

$$C_s \in [C_s^{\min}, C_s^{\max}] \cdot U_s \quad (3b)$$

$$W_s \leq C_s \cdot C_{\text{rate}} \quad (3c)$$

The set of constraints  $\Lambda(\Omega_2)$  includes the SOC-OPF grid constraints in [15] (4)<sup>4</sup> and BESSs operational constraints (5). (4k) constitutes the tightness-promoting constraint, under the hypotheses (4l). (5b) and (5c) enforce day-ahead energy and balancing power market neutrality, respectively. For brevity, nodal voltage magnitudes and angles, and generator reactive-power limits, are omitted; all constraints are understood to hold for every index in the corresponding sets. The parameters  $A_{nl}^+$ ,

<sup>1</sup>A daily decomposition mirrors day-ahead operation and enforces BESS state-of-energy continuity over each 24-hour horizon.

<sup>2</sup>The SOC relaxation of the OPF in [15] replaces the branch reactive power balance equality with an inequality (4h). See Section IV-C for further details.

<sup>3</sup>A lossless battery model is assumed. Losses can be incorporated while preserving convexity of the problem [29].

<sup>4</sup>For brevity, PST and OLTC models are omitted; importantly, phase-shift and tap-ratio variables can be included linearly in the PF equations.

$A_{nl}^-$ ,  $G_n$ ,  $B_n$ ,  $R_l$ , and  $X_l$  are defined in [15]. The matrices  $A_{s_l n}$  and  $A_{r_l n}$  are branch-to-node incidence matrices, with entries equal to 1 at the sending and receiving end of branch  $l$ , respectively.

$$p_{n,t} = \sum_{l \in \mathcal{L}} (A_{nl}^+ p_{s_l,t} - A_{nl}^- p_{o_l,t}) + G_n V_{n,t} \quad (4a)$$

$$q_{n,t} = \sum_{l \in \mathcal{L}} (A_{nl}^+ q_{s_l,t} - A_{nl}^- q_{o_l,t}) - B_n V_{n,t} \quad (4b)$$

$$p_{n,t} = P_{n_g,t} - P_{n_s,t} - P_{n_l,t} \quad (4c)$$

$$q_{n,t} = Q_{n_g,t} - Q_{n_s,t} - Q_{n_l,t} \quad (4d)$$

$$(A_{s_l n} - A_{r_l n}) V_{n,t} = 2R_l p_{s_l,t} + 2X_l q_{s_l,t} - R_l p_{o_l,t} - X_l q_{o_l,t} \quad (4e)$$

$$\theta_{l,t} = X_l p_{s_l,t} - R_l q_{s_l,t} \quad (4f)$$

$$\theta_{l,t} = (A_{s_l n} - A_{r_l n}) \theta_{n,t} \quad (4g)$$

$$q_{o_l,t} \geq \frac{p_{s_l,t}^2 + q_{s_l,t}^2}{V_{s_l,t}} X_l \quad (4h)$$

$$K_{o_l,t} \geq q_{o_l,t} \quad (4i)$$

$$p_{o_l,t} X_l = q_{o_l,t} R_l \quad (4j)$$

$$(A_{s_l n} V_{n,t})(A_{r_l n} V_{n,t}) \sin^2(\theta_l^{\max}) \geq \theta_{l,t}^2 \quad (4k)$$

$$(\theta_l^{\min}, \theta_l^{\max}) \subseteq \left(-\frac{\pi}{2}, \frac{\pi}{2}\right), \quad \theta_l^{\min} = -\theta_l^{\max} \quad (4l)$$

$$E_{s,t+1} = E_{s,t} + P_{n_s,t} \Delta t \quad (5a)$$

$$E_{s,t^i} = E_{s,t^f} \quad (5b)$$

$$\sum_{s \in \mathcal{S}} P_{s,t} = 0 \quad (5c)$$

The constraints involving linking variables  $\Xi(\Omega_1, \Omega_2)$  include the storage converter capability curve <sup>5</sup> (6a), the state-of-energy limits (6b) and continuity boundary conditions (6c).

$$W_s^2 \geq P_{n_s,t}^2 + Q_{n_s,t}^2 \quad (6a)$$

$$E_{s,t} \in [SoE^{\min}, SoE^{\max}] \cdot C_s \quad (6b)$$

$$E_{s,t^i} = 0.5 \cdot (SoE^{\max} - SoE^{\min}) \cdot C_s \quad (6c)$$

When decomposed, the main problem takes the form

$$(\text{MP}) : \min_{\Omega_1, \alpha_d} \frac{1}{\tau} \cdot \text{CAPEX} + \sum_{d \in \mathcal{D}} \alpha_d \quad (7a)$$

s.t.

$$\Pi(\Omega_1) \leq 0 \quad (7b)$$

$$\alpha_d \geq \underline{\alpha}, \forall d \in \mathcal{D} \quad (7c)$$

$$\alpha_d \geq \Gamma_d^{(\beta)}, \forall (d, \beta) \in \Phi \quad (7d)$$

$$\Upsilon_d^{(\beta)} \leq 0, \forall (d, \beta) \in (\mathcal{D} \times \mathcal{B}) \setminus \Phi \quad (7e)$$

with  $\alpha_d$  proxy variable for the operational cost of subproblem  $d \in \mathcal{D}$ ,  $\mathcal{B} = \{1, \dots, k-1\}$  set of completed Benders iterations, with  $k$  denoting the current iteration and  $\Phi := \{(d, \beta) \in \mathcal{D} \times \mathcal{B} \mid \text{subproblem } d \text{ is feasible at iteration } \beta\}$  set of feasible subproblems across Benders iterations. As the algorithm progresses, optimality cuts (7d) and feasibility cuts (7e) are iteratively added to the set of constraints. The

---

### Algorithm 1 Generalized Benders Decomposition

---

- 1: Initialize  $\underline{\alpha}_d = 0$ , set iteration counter  $k = 1$ .
  - 2: **Step 1: main problem**
  - 3: Solve (MP) and compute  $LB^{(k)}$ .
  - 4: Pass the optimal linking-variable  $\hat{W}_s, \hat{C}_s$  values to all subproblems.
  - 5: **Step 2: Subproblem stage**
  - 6: **for all**  $d \in \mathcal{D}$  **do**
  - 7:     **if** subproblem  $d$  is feasible **then**
  - 8:         Solve (SBP) <sub>$d$</sub>  and compute  $\Gamma_d^{(k)}$ .
  - 9:         Update  $\Phi \leftarrow \Phi \cup \{(d, k)\}$ .
  - 10:     **else**
  - 11:         Solve (FC-SBP) <sub>$d$</sub>  and compute  $\Upsilon_d^{(k)}$ .
  - 12:     **end if**
  - 13: **end for**
  - 14: Compute  $UB^{(k)}$ .
  - 15: **Step 3: Convergence check**
  - 16: **if** all  $d \in \mathcal{D}$  feasible **and**  $|UB^{(k)} - LB^{(k)}| / LB^{(k)} < \varepsilon$  **then**
  - 17:     Solve the non-approximated AC-PF, with as input the optimal operating point.
  - 18:     **Output:** optimal linking-variables, state variables and total cost from the PF.
  - 19: **else**
  - 20:      $k \leftarrow k + 1$ .
  - 21:     Go to **Step 1**.
  - 22: **end if**
- 

right-hand-sides of these linear inequalities take the form (9) and (11), and are derived from the subproblem (8) and the feasibility check subproblem (10), respectively.

$$(\text{SBP})_d : \min_{\Omega_1, \Omega_2} \text{OPEX}_d \quad (8a)$$

s.t.

$$\Lambda(\Omega_2) \leq 0 \quad (8b)$$

$$\Xi(\Omega_1, \Omega_2) \leq 0 \quad (8c)$$

$$W_s = \hat{W}_s \quad : \lambda_{s,d} \quad (8d)$$

$$C_s = \hat{C}_s \quad : \mu_{s,d} \quad (8e)$$

$$\Gamma_d^{(\beta)} = \overline{\text{OPEX}}_d^{(\beta)} + \sum_{s \in \mathcal{S}} \bar{\lambda}_{s,d}^{(\beta)} (W_s - \hat{W}_s^{(\beta)}) + \sum_{s \in \mathcal{S}} \bar{\mu}_{s,d}^{(\beta)} (C_s - \hat{C}_s^{(\beta)}) \quad (9)$$

$$(\text{FC-SBP})_d : \min_{\Omega_1, \Omega_2, s_{W_s}, s_{C_s}} w_{\text{slack}} \sum_{s \in \mathcal{S}} (s_{W_s} + s_{C_s}) \quad (10a)$$

s.t.

$$\Lambda(\Omega_2) \leq 0 \quad (10b)$$

$$\Xi(\Omega_1, \Omega_2) \leq 0 \quad (10c)$$

$$W_s = \hat{W}_s + s_{W_s} \quad : \nu_{s,d} \quad (10d)$$

$$C_s = \hat{C}_s + s_{C_s} \quad : \xi_{s,d} \quad (10e)$$

$$s_{W_s}, s_{C_s} \geq 0 \quad (10f)$$

<sup>5</sup>Assuming BESSs converter P/Q limits are voltage independent.

$$\Upsilon_d^{(\beta)} = w_{\text{slack}} \sum_{s \in \mathcal{S}} \left( \tilde{s}_{W_s, d}^{(\beta)} + \tilde{s}_{C_s, d}^{(\beta)} \right) + \sum_{s \in \mathcal{S}} \tilde{\nu}_{s, d}^{(\beta)} \left( W_s - \hat{W}_s^{(\beta)} \right) + \sum_{s \in \mathcal{S}} \tilde{\xi}_{s, d}^{(\beta)} \left( C_s - \hat{C}_s^{(\beta)} \right) \quad (11)$$

Throughout this formulation, the operator  $\hat{(\cdot)}$  denotes the optimal variables output of the main problem,  $(\cdot)$  of the subproblems, and  $\tilde{(\cdot)}$  of the feasibility check subproblems.

The lower bound on the total cost is computed as  $LB^{(k)} = \frac{\gamma}{\tau} \text{CAPEX}^{(k)} + \sum_{d \in \mathcal{D}} \hat{\alpha}_d^{(k)}$ ,  $k$  current Benders iteration, and its upper bound as  $UB^{(k)} = \frac{\gamma}{\tau} \text{CAPEX}^{(k)} + \sum_{d \in \mathcal{D}} \overline{\text{OPEX}}_d^{(k)}$ .

2) *Computational complexity and parallel solution approach*: The optimization framework is implemented in CVXPY [30] and solved using the MOSEK [12] conic optimizer. Each subproblem is constructed with parametrized linking variables and “dummy-solved” once to trigger compilation and caching.<sup>6</sup> This initialization stage is executed sequentially on a single process. Afterwards, at each iteration, subproblems are distributed across all available CPU cores and solved in parallel. Model construction is decoupled from model evaluation<sup>7</sup>, to keep memory usage bounded and substantially reduce total run time.

TABLE I  
CENTRALIZED PROBLEM SIZE.

Centralized	
Var (bin)	$S$
Var (cont)	$(2 + G + 4N + 6L)T + (2T + (T + 1) + 2)S$
Cons	$(7 + 2G + 8N + 10L)T + (2T + 2(T + 1) + 6 + 2D)S$

TABLE II  
DECOMPOSED PROBLEM SIZE.

	MP	SBP
Var (bin)	$S$	0
Var (cont)	$2S + D$	$(2 + G + 4N + 6L)P + (2P + (P + 1) + 2)S$
Cons	$5S + D( \mathcal{B}  + 1)$	$(7 + 2G + 8N + 10L)P + (2P + 2(P + 1) + 5)S$
Par	0	$2S$

TABLE III  
CENTRALIZED VS. DECOMPOSED PROBLEM SIZES, FOR THE IEEE 118-BUS SYSTEM.

	Centralized	Decomposed	
		MP	SBP
Var (bin)	118	118	0
Var (cont)	17126154	260	47274
Cons	29161524	$590 + 24( \mathcal{B}  + 1)$	80482
Par	0	0	236

The sizes of the centralized and of the decomposed formulation are reported in Table I and Table II, respectively<sup>8,9</sup>. The subproblem size is reported per instance; total counts in

<sup>6</sup>The first `solve` call checks DCP compliance, canonicalizes the model into a cone program, builds the solver data, and caches the compiled representation.

<sup>7</sup>At each iteration, only the coefficient entries affected by the linking parameters are updated before the conic solver is called.

<sup>8</sup> $G := |\mathcal{G}|$ ,  $N := |\mathcal{N}|$ ,  $L := |\mathcal{L}|$ ,  $S := |\mathcal{S}|$ ,  $T := |\mathcal{T}|$ ,  $D := |\mathcal{D}|$ ,  $P := |\mathcal{P}|/|\mathcal{D}|$ .

<sup>9</sup>“Var (bin)” and “Var (cont)” denote binary and continuous variables; “Par” denotes parameters and “Cons” constraints, following CVXPY’s terminology.

Table II and III, column “SBP” scale with the number of subproblems (or, under parallel execution, with the number of concurrently solved instances). Notably, subproblem dimensions remain constant across Benders iterations. In contrast, the main-problem size grows linearly with the iteration count  $|\mathcal{B}|$ , since one cut per subproblem is generated and retained at each iteration.

Notably, the subproblem dimensions remain constant across Benders iterations. In contrast, the main problem size grows linearly with the iteration count  $|\mathcal{B}|$ , since one cut per subproblem is generated and retained at each Benders iteration. For the IEEE 118-bus system (namely, the test network used in the case study) over a one-year horizon, the corresponding numerical sizes are reported in Table III.

3) *Convergence*: The work in [28] extends the GBD framework to MINLP with vector conic constraints in Banach spaces, providing the theoretical basis for optimality and feasibility cuts formulation through a generalized version of Farkas’ lemma. The geometric interpretation of the lemma is that a vector either lies in the cone or can be strictly separated from it by a hyperplane. In GBD, this result provides a certificate of infeasibility and underpins the formulation of the feasibility-check subproblem, that is a numerical procedure to compute such a separating hyperplane.

In the present setting, the hypothesis in [26] that the main problem feasible set be finite is not satisfied, since the main problem includes both (site) binary variables and (size) continuous variables. Nevertheless, convergence guarantees remain valid; see Appendix A for a formal argument.

Moreover, unlike existing formulations (e.g., [28], [31]), slack variables are introduced in the feasibility-check subproblem *only* for the linking variables (10d), (10e), rather than for every constraint. This remains consistent with Farkas’ lemma provided that the slack variables enter the conic constraints linearly, thereby preserving the theoretical convergence guarantees of GBD. A formal justification is provided in Appendix A.

Finally, note that the subproblems (8) solve convex relaxations of the original AC-OPF. In the feasibility-check subproblem, the Farkas’ lemma requires an objective that penalizes only the slack variables (losses cannot be included to promote tightness, as is common in standard SOC-OPF formulations). Consequently, the feasibility-check subproblem might return an operating point that differs from the regular subproblem and slow convergence: part of the infeasibility may be absorbed through the artificially inflated losses permitted by the relaxation, rather than being reflected solely in the slack variables. Nevertheless, the algorithm’s convergence guarantees remain unaffected.

## B. Second-order cone relaxation of the optimal power flow

*Tightness*: The SOC-OPF model adopted here follows [15], which explicitly models bus voltage angles and advocates applicability to both radial and meshed topologies. However, the authors of this paper argue that tightness cannot be formally guaranteed for meshed networks. This issue is discussed in further detail in another work by the authors [32], where this limitation is formally established and supported by

experimental evidence showing that, even with a numerically zero total relaxation gap, substituting the relaxed solution into the nonlinear AC-PF equations yields nonzero residuals on IEEE test networks.

Briefly, constraint (4f) in the SOC-OPF formulation of [15] is derived by approximating the AC-OPF-feasible equation (12),

$$v_{sl}v_{rl}\sin(\theta_{l,t}) = X_l p_{sl,t} - R_l q_{sl,t}, \quad (12)$$

and the cyclic constraint (13) is claimed to hold when (4g) is included in the set of constraints

$$\sum_{l \in \mathcal{C}} \theta_l = 0 \bmod 2\pi, \quad \forall \mathcal{C} \text{ cycle.} \quad (13)$$

Lemma 1 in [32] shows that this implication does not hold in general. Moreover, the monotonic load-increase procedure required to promote tightness in Theorems 5 and 6 of [15] is not admissible in the context of this work, since load injections are fixed parameters. For this reason, a semi-heuristic procedure is adopted to recover an AC-PF-feasible solution to the planning problem. Specifically, once the algorithm has converged, an AC-PF is solved using the state variables obtained from the SOC-OPF (see Stage 17 in Algorithm 1).

#### IV. CASE STUDIES AND RESULTS

The simulations are carried out on a MacBook Pro equipped with an Apple M4 Pro chip featuring 10 efficiency cores and 48 GB of RAM.

The IEEE 118-bus network [33] is used as test system. Time-series profiles (hourly) of nodal active power net injections (generation minus load) are sourced from IEEE DataPort<sup>10</sup>. These injections are derived from a DC-PF, and therefore neglect reactive power and losses. To obtain physically meaningful active and reactive injections for the planning problem, an AC-PF initialization is performed. Specifically, load power factors are computed for all PQ buses and for buses hosting only synchronous condensers using the snapshot operating-point values in the MATPOWER case file<sup>11</sup>. Reactive injections at these buses are then reconstructed from the time-series active power and the corresponding power factors. For synchronous generator buses, the time-series data does not distinguish load from generation; therefore, the reactive component of the local load is approximated using the load profile of the PQ bus whose power factor is closest to the nominal MATPOWER value.

The AC-PF is then solved using the reconstructed  $P$ - $Q$  injections, a flat-start (i.e. nodal voltage magnitudes set to 1, and phases to 0) initialization for PV-bus voltages, and reactive power limits from the MATPOWER case file. Over the selected time horizon, the resulting operating points exhibit voltage-magnitude violations at twelve buses, and the slack generator exceeds both active and reactive power limits. These injections serve as input to the optimal BESS allocation problem, which seeks to resolve voltage and ampacity violations. To explicitly induce congestion, additional infeasibilities are

introduced by tightening selected line ampacity limits. Specifically, buses with voltage violations are selected as candidate battery locations and the ampacity limits of lines incident to these buses are reduced so that the network becomes infeasible in the absence of storage. In contrast, slack-bus active power limits are relaxed, since this infeasibility cannot be addressed by storage constrained to have equal state of energy at the beginning and end of each day. These boundary conditions are illustrated in Figure 1. Before evaluating the proposed framework for the optimal BESS allocation problem, three preliminary studies are performed: (i) verification of GBD convergence to the centralized solution, (ii) analysis of GBD solve-time scalability with respect to the planning horizon and the number of candidate battery locations, and (iii) assessment of the tightness of the relaxed grid constraints.

#### A. Generalized Benders Decomposition convergence

The planning problem is a non-convex MISOCP. Consequently, neither the centralized formulation nor its Benders-decomposed counterpart provides guarantees of global optimality. To verify the correctness of the decomposed formulation, two sets of boundary conditions, tailored to isolate the generation of (1) optimality and (2) feasibility cuts, are considered.

To test the optimality-cut mechanism, the binary variables are relaxed, obtaining a centralized convex SOCP. In this setting, GBD is guaranteed to converge to the global optimum of the relaxation and thus to the centralized solution. All operational infeasibilities are removed<sup>12</sup> to ensure that subproblems generate optimality cuts only. To validate feasibility cuts, the finite-convergence assumptions in [26] requiring polyhedral subproblem feasible sets are exploited. The SOC-OPF grid constraints in the subproblems are therefore replaced with a DC-OPF, yielding linear programming (LP) subproblems, which combined with a LP main problem, produce a centralized LP. In this second setting, infeasibilities in the boundary conditions (voltage violations and line congestions) are included so that feasibility cuts are generated.

Figure 2 reports the residuals of state variables<sup>13</sup> (left) and linking variables (right) between the centralized and decomposed solutions in the feasible setting, for four representative days<sup>14</sup> and for different weights on power losses in the subproblem objective. The GBD termination criterion is set to  $(UB - LB) < \delta$  with  $\delta = 1e-1$  p.u. (instead of Stage 16 in Algorithm 1) to control the accuracy with respect to the linking-variable decisions and to avoid an explicit dependence on the loss weight magnitude. The corresponding value of  $\varepsilon$  in Stage 16 of Algorithm 1, computed *a posteriori*, is  $1e-2$ ,  $1e-4$ , and  $1e-6$  for the three tested loss weights, respectively. Two opposite trends are observed: state-variable residuals are

<sup>12</sup>Voltage-magnitude limits and slack-bus active power constraints are relaxed.

<sup>13</sup> $\tilde{p}_{s_l}, \tilde{q}_{s_l}$  are the measurable active and reactive power at the sending end  $s$  of branch  $l$ , see [15] for further details.

<sup>14</sup>The four representative days are selected based on the seasonal variation of the daily active power profile of the PQ bus with the largest load. Daily profiles are clustered by season (Dec–Jan–Feb, Mar–Apr–May, Jun–Jul–Aug, Sep–Oct–Nov), and the day with minimum RMSE with respect to the seasonal median is chosen as representative.

<sup>10</sup><https://ieee-dataport.org/documents/time-series-data-load-generation-and-power-flow-ieee-bus-systems>

<sup>11</sup><https://matpower.org/docs/ref/matpower5.0/case118.html>

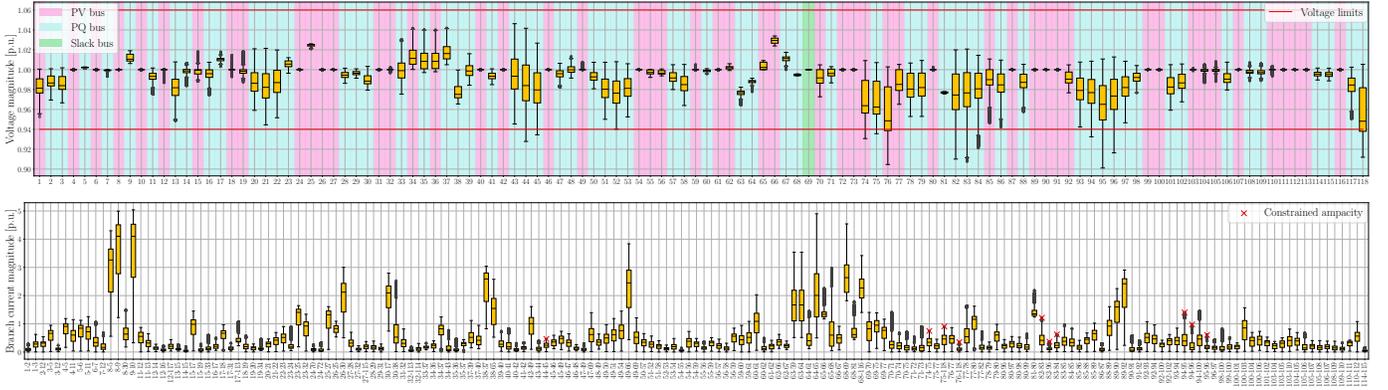


Fig. 1. Boundary conditions: distribution of voltage (top) and branch current (bottom) magnitude over the time horizon, per bus and branch respectively.

largest for small loss weights, whereas linking-variable residuals are smallest. As the loss weight increases, the operational term dominates the objective and the relative contribution of the size variables becomes marginal; consequently, for large loss weights, even if state-variable residuals are negligible, indicating matching operating points, linking-variable residuals approach the termination tolerance. Overall, the near-zero (or tolerance-level) residuals obtained for  $C_s$  and  $W_s$  for a unitary loss weight support the correct implementation of the optimality cuts within GBD. Analogously, Figure 3 reports the

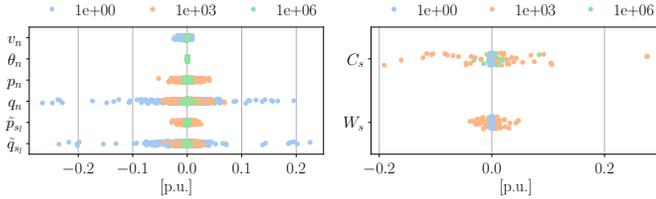


Fig. 2. Residuals between the optimal solutions of the centralized and Benders-decomposed integrality-relaxed problem: feasible setting. SOC-OPF state variables (left) and linking variables (right).

residuals of the same quantities for the infeasible boundary conditions. Here, the variable weight is on the slack bus power in the subproblem objective. The termination threshold is set to  $\delta = 1e-2$ , which leads to  $\varepsilon = 1e-8$ . Again, near-zero (or tolerance-level) residuals of the linking variables for small subproblem objective weights support the correct implementation of feasibility cuts.

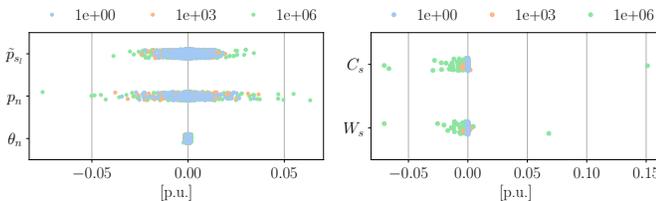


Fig. 3. Residuals between the optimal solutions of the centralized and Benders-decomposed integrality-relaxed problem: infeasible setting. DC-OPF state variables (left) and linking variables (right).

### B. Solution time and scalability

The next simulations evaluate the computational performance of the GBD algorithm applied to the non-convex

MISOCP. Here, “convergence” refers to termination of the algorithm in a finite number of iterations; it does not imply global optimality, nor equality to the centralized solution.

Figure 4 illustrates the scalability of the proposed framework with respect to the number of subproblems (i.e., the planning horizon length) (left) and the number of linking variables (battery size variables) (right), both varied geometrically. The termination tolerance is set to  $\varepsilon = 1e-4$  and  $1e-2$ , respectively.

Concerning the number of subproblems, consistently with the discussion on computational complexity in Section III-A2, the main problem solve time exhibits an approximately linear dependence on the planning horizon length<sup>15</sup>. Its dispersion across iterations is non-negligible and is further evidenced in Figure 5 (left), which shows an increasing main problem solve time as a function of the Benders iteration index due to the accumulation of cuts. For the subproblems, the cumulative per-iteration solve time grows linearly with the number of subproblems (for number of subproblems  $\geq 9$ ), with a proportionality constant close to the number of available parallel workers (CPU cores), whereas the per-iteration maximum solve time across workers plateaus. Finally, the number of iterations required for termination remains approximately constant or decreases (cf. Figure 5 (right)), which is consistent with the fact that increasing the number of subproblems yields more cuts per iteration and therefore restricts the main-feasible region more rapidly.

Concerning the number of linking variables, the main problem solve time increases more than linearly, as the main is a MILP whose integer dimension scales with the number of candidate locations. In contrast, the subproblem solve time per iteration remains approximately constant. The number of Benders iterations grows rapidly with the number of linking variables, indicating that the algorithmic effort required for termination increases markedly as the dimension of the binary and linking-variable space grows. This constitutes the main practical limitation of the approach. A closed-form scaling law is not reported, as the observed iteration growth is strongly affected by the spatial distribution of candidate locations.

<sup>15</sup>A log-log linear fit of the form  $\log_{10} y = m \log_{10} x + q$  yields  $m \approx 0.9$ , i.e., close to the ideal linear scaling ( $m = 1$ ), and  $10^q \approx 0$ .

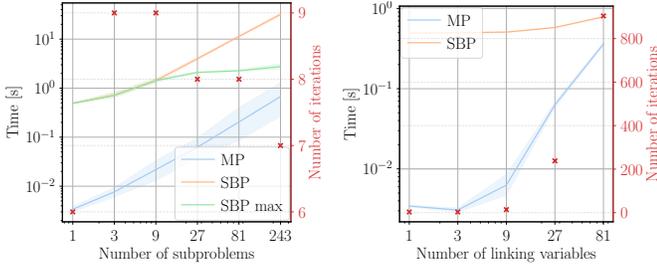


Fig. 4. Main-problem solve time per iteration (blue), total subproblem solve time per iteration (orange), maximum subproblem solve time across workers (green) and number of Benders iterations (red) as functions of the number of subproblems (left) and number of linking variables (right). Mean (solid line) and standard deviation (shaded area) across iterations.

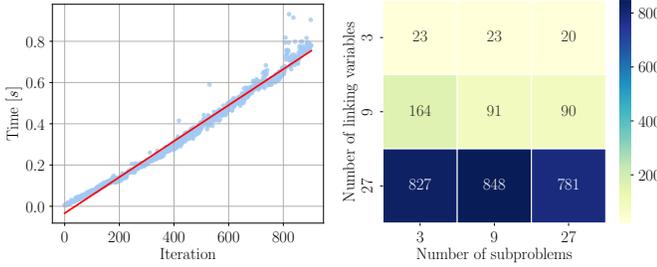


Fig. 5. Main problem solve-time per iteration as a function of Benders iteration count (left) and number of Benders iterations as a joint function of number of subproblems and linking variables (right).

Overall, Table IV and Table V report the total solution time for the main problem and subproblems at termination, confirming the computational efficiency of the approach. The dominant contributors to overall runtime are, in decreasing order, the number of linking variables, the termination tolerance (which drives the iteration count), and the number of subproblems, which is partly mitigated by parallelization. In practice, this suggests that long planning horizons are computationally tractable, whereas the number of candidate BESS locations should be kept moderate.

TABLE IV

MAIN (MP) AND SUBPROBLEM (SBP) TOTAL SOLUTION TIME AS A FUNCTION OF THE NUMBER OF SUBPROBLEMS.

# days	1	3	9	27	81	243	365
MP [s]	0.05	0.07	0.18	0.45	1.44	4.05	7.35
SBP [s]	2.94	17.94	108.80	293.69	867.69	2193.81	5192.92

TABLE V

MAIN (MP) AND SUBPROBLEM (SBP) TOTAL SOLUTION TIME AS A FUNCTION OF THE NUMBER OF LINKING VARIABLES.

# linking variables	1	3	9	27	81	118
MP [s]	0.04	0.02	0.09	14.91	325.34	3432.16
SBP [s]	1.48	1.50	7.11	137.86	711.21	1972.77

### C. Tightness and AC-power flow feasibility

Tightness of the SOC-OPF relaxation is commonly assessed via the relaxation gap. A zero gap is not generally guaranteed when loads are fixed, and the aggregate gap magnitude alone

is not a reliable metric of proximity to an AC-PF-feasible operating point. As shown in Figure 6 (left), the relaxation gap obtained with a linear loss penalty is very small (on the order of  $1e-6 \div 1e-7$  p.u.); nonetheless, the nodal active/reactive power residuals in Figure 6 (right) (obtained by evaluating the nonlinear AC-PF equations at the optimized voltage magnitudes and angles) indicate that the resulting operating point is not feasible. Under a linear loss penalty, the gap tends to concentrate on a limited subset of branches, where artificially inflated losses incur the lowest marginal cost. This may violate cycle constraints on voltage phase angles and thereby yield AC-infeasible solutions. To partially mitigate this effect, a

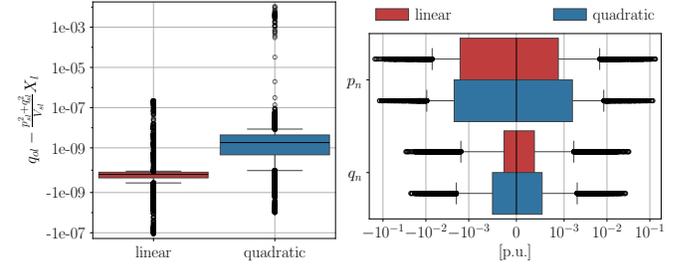


Fig. 6. Distribution of the relaxation gap on reactive power losses over the time horizon (left), and nodal power residuals between the optimization solution and the AC-PF equations evaluated at the optimized voltage phasors (right), for linear (red) and quadratic (blue) loss costs.

more distributed penalty is considered, implemented as a quadratic cost on reactive power losses. While this objective spreads the gap more evenly across branches (as reflected by a wider interquartile range and outliers reaching  $1e-2$  [p.u.]), it provides only limited improvements in AC consistency: the maximum nodal residuals remain on the order of  $10^{-1}$  p.u. in Figure 7<sup>16</sup>.

These observations motivate a final refinement step, in which an AC-PF is solved using the optimization output as initialization. Mean, median and maximum AC-PF solution times per time step (with reactive-limit checks) are respectively 0.0906 s, 0.0892 s, and 0.1396 s confirming that the refinement step remains computationally tractable across all considered horizons. Finally, since in the decomposed scheme subprob-

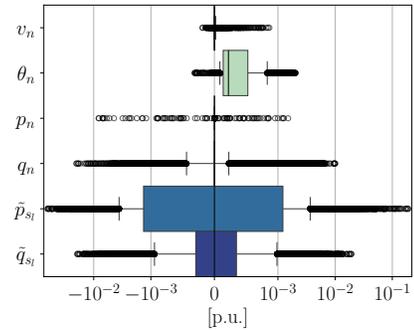


Fig. 7. Residuals between the optimization solution and the AC-PF solved using the optimization solution as initialization.

lems are solved independently of the main problem, tightness can be promoted without careful tuning of loss-penalty

<sup>16</sup>Residuals are reported in per unit on a common 100 MW base.

weights, while preserving an interpretable cost structure for storage investment. In contrast, centralized formulations often require disproportionately large weights on losses for them to dominate the objective [7].

#### D. Optimal siting and sizing

As a final simulation, the proposed framework is tested in a typical TSO setting. The planning horizon spans 365 days, the candidate BESS locations are restricted to the 12 buses exhibiting voltage magnitude violations and the ampacity limits are set to 82% of the maximum branch current achieved in the results of the PF for the branches with candidate battery locations at both ends (10 in total). The convergence threshold is set to  $\varepsilon = 5e-3$ , weights to  $w_{\text{loss}} = 1$ , and  $w_{\text{slack}} = 1e+3$ . Without loss of generality, costs are unitary  $IC_s^{\text{power}} = IC_s^{\text{energy}} = 1$  CHF/W and CHF/W h,  $\forall s$ ,  $OC_l = 1$  CHF/W<sup>2</sup>,  $\forall l$ . Table VI reports the resulting optimal siting and sizing decisions together with the corresponding objective value. The algorithm terminates in 148 Benders iterations, for a total solution time of 16 145 s (less than 5 h). Infeasibility is manifested in 39 subproblems and feasibility is finally restored after iteration 143 out of 147. The total time spent solving the power flow once convergence is achieved is 974 s and tightness is of the same order of magnitude of Figure 7.

TABLE VI  
TOTAL NUMBER OF INSTALLED BATTERIES, THEIR RATED POWER AND ENERGY, CAPEX AND OPEX.

$\sum_{s \in \mathcal{S}} U_s$	$\sum_{s \in \mathcal{S}} W_s$	$\sum_{s \in \mathcal{S}} C_s$	CAPEX	OPEX
12	1576 MW	5488 MW h	70.6 CHF	10980.3 CHF

#### V. CONCLUSION

In conclusion, the proposed framework enables the computationally tractable solution of high-resolution, operationally driven BESS allocation problems over annual (and, in principle, multi-year) horizons on large-scale meshed transmission networks. By reformulating the planning task as a MISOCP and solving it via a parallelized GBD scheme, solution times are reduced to the range of minutes to hours (depending on the boundary conditions) even on portable hardware. The formulation is general and can be specialized to different operational objectives (in this work, efficiency is targeted under voltage- and ampacity-limit infeasibilities), and features rigorous convergence guarantees. Moreover, an AC-PF-feasible operating point can be recovered from the relaxed solution at modest additional computational cost. Scalability results indicate that long horizons are primarily limited by available parallelism, whereas the dominant bottleneck is the number of linking variables, motivating a sparse candidate BESS locations set, an assumption that is often consistent with practical planning tasks.

Overall, the framework supports TSOs considering the procurement of BESS as grid-support assets: with market-cleared net injections as input, it enables congestion management and voltage regulation with TSO-controlled resources that are constrained to be market-neutral, potentially reducing the need for costly remedial actions.

Future work will extend the assessment to larger, real-world (non-synthetic) transmission networks, include  $N - 1$  security assessment and broaden scalability studies, including scenario variability and stochastic formulations.

#### REFERENCES

- [1] Z. Zhao, Y. Shang, B. Qi, Y. Wang, and Q. Zhang, "Optimal sizing and siting of energy storage systems based on power grid vulnerability analysis: a trilevel optimization model," *Energy Strategy Reviews*, vol. 59, p. 101720, 2025.
- [2] J. Qiu, Z. Xu, Y. Zheng, D. Wang, and Z. Y. Dong, "Distributed generation and energy storage system planning for a distribution system operator," *IET Renewable Power Generation*, vol. 12, no. 12, pp. 1345–1353, 2018.
- [3] X. Shen, M. Shahidepour, Y. Han, S. Zhu, and J. Zheng, "Expansion planning of active distribution networks with centralized and distributed energy storage systems," *IEEE Transactions on Sustainable Energy*, vol. 8, 2016.
- [4] H. Pandžić, Y. Wang, T. Qiu, Y. Dvorkin, and D. S. Kirschen, "Near-optimal method for siting and sizing of distributed storage in a transmission network," *IEEE Transactions on Power Systems*, vol. 30, no. 5, pp. 2288–2300, 2015.
- [5] S. Massucco, P. Pongiglione, F. Silvestro, M. Paolone, and F. Sossan, "Siting and sizing of energy storage systems: Towards a unified approach for transmission and distribution system operators for reserve provision and grid support," *Electric Power Systems Research*, vol. 190, p. 106660, 2021.
- [6] M. Asensio, P. Meneses de Quevedo, G. Muñoz-Delgado, and J. Contreras, "Joint distribution network and renewable energy expansion planning considering demand response and energy storage—part i: Stochastic programming model," *IEEE Transactions on Smart Grid*, vol. 9, no. 2, pp. 655–666, 2018.
- [7] J. H. Yi, R. Cherkaoui, M. Paolone, D. Shchetinin, and K. Knezovic, "Optimal co-planning of esss and line reinforcement considering the dispatchability of active distribution networks," *IEEE Transactions on Power Systems*, vol. 38, no. 3, pp. 2485–2499, 2023.
- [8] M. Nick, R. Cherkaoui, and M. Paolone, "Optimal allocation of dispersed energy storage systems in active distribution networks for energy balance and grid support," *IEEE Transactions on Power Systems*, vol. 29, no. 5, pp. 2300–2310, 2014.
- [9] A. Hassan and Y. Dvorkin, "Energy storage siting and sizing in coordinated distribution and transmission systems," *IEEE Transactions on Sustainable Energy*, vol. 9, no. 4, pp. 1692–1701, 2018.
- [10] N. J. Higham, *Accuracy and Stability of Numerical Algorithms*, 2nd ed. Society for Industrial and Applied Mathematics (SIAM), 2002.
- [11] Gurobi Optimization, LLC, "Gurobi Optimizer Reference Manual," 2026. [Online]. Available: <https://www.gurobi.com>
- [12] MOSEK ApS, "MOSEK Optimizer API for Python 11.0.30," 2019. [Online]. Available: <https://docs.mosek.com/latest/pythonapi/index.html>
- [13] P. Panciatici, M. Campi, S. Garatti, S. Low, D. Molzahn, A. Sun, and L. Wehenkel, "Advanced optimization methods for power systems," in *2014 Power Systems Computation Conference*, 2014, pp. 1–18.
- [14] M. Farivar and S. H. Low, "Branch flow model: Relaxations and convexification—part i," *IEEE Transactions on Power Systems*, vol. 28, no. 3, pp. 2554–2564, 2013.
- [15] Z. Yuan and M. Paolone, "Properties of convex optimal power flow model based on power loss relaxation," *Electric Power Systems Research*, vol. 186, p. 106414, 2020.
- [16] H. Kim, S. Lee, S. Han, W. Kim, K. Ok, and S. Cho, "Integrated generation and transmission expansion planning using generalized bender's decomposition method," in *2015 IEEE International Conference on Computational Intelligence & Communication Technology*, 2015, pp. 493–497.
- [17] P. Eguía, E. Torres, A. Etxegarai, V. Valverde, and I. Zamora, "Optimum allocation of bess for power quality improvement. a comparative study," in *2019 International Conference on Clean Electrical Power (ICCEP)*, 2019, pp. 450–455.
- [18] J. H. Yi, "Dispatch-aware optimal planning of active distribution networks including energy storage systems," PhD thesis, EPFL, Lausanne, 2023.
- [19] D. Chen, Z. Jing, and H. Tan, "Optimal siting and sizing of used battery energy storage based on accelerating benders decomposition," *IEEE Access*, vol. 7, pp. 42993–43003, 2019.
- [20] A. J. Conejo, E. Castillo, R. Múñez, and R. García-Bertrand, *Decomposition Techniques in Mathematical Programming*, 1st ed. Springer Berlin, Heidelberg, 2006.

- [21] J. C. López, M. Granada, and J. R. S. Mantovani, "Multi-area decentralized optimal var planning using the dantzig-wolfe decomposition principle," in *2010 IEEE/PES Transmission and Distribution Conference and Exposition: Latin America (T&D-LA)*, 2010, pp. 92–98.
- [22] A. S. Zamzam, E. Dall'Anese, and N. D. Sidiropoulos, "Optimal distributed energy storage management using relaxed dantzig-wolfe decomposition," in *2018 IEEE Conference on Decision and Control (CDC)*, 2018, pp. 2396–2401.
- [23] Y. Wu, L. Yao, S. Liao, and B. Mao, "Distributed optimal scheduling of integrated energy system based on admm algorithm," in *2021 IEEE Sustainable Power and Energy Conference (iSPEC)*, 2021, pp. 902–906.
- [24] J. Chen, K. Li, H. Wang, D. Zhao, C. Jiang, and C. Zhang, "Distributed parallel optimal operation for shared energy storage system - multiple park integrated energy system based on admm," *Energy*, vol. 317, p. 134677, 2025.
- [25] J. F. Benders, "Partitioning procedures for solving mixed-variables programming problems," *Numerische Mathematik*, vol. 4, no. 1, pp. 238–252, 1962.
- [26] A. M. Geoffrion, "Generalized benders decomposition," *Journal of Optimization Theory and Applications*, vol. 10, no. 4, pp. 237–260, 1972.
- [27] N. Sahinidis and I. Grossmann, "Convergence properties of generalized benders decomposition," *Computers & Chemical Engineering*, vol. 15, no. 7, pp. 481–491, 1991.
- [28] Z. Wei and M. M. Ali, "Generalized benders decomposition for one class of minlps with vector conic constraint," *SIAM Journal on Optimization*, vol. 25, no. 3, pp. 1809–1825, 2015.
- [29] E. Stai, L. Reyes-Chamorro, F. Sossan, J.-Y. Le Boudec, and M. Paolone, "Dispatching stochastic heterogeneous resources accounting for grid and battery losses," *IEEE Transactions on Smart Grid*, vol. 9, no. 6, pp. 6522–6539, 2018.
- [30] A. Agrawal, R. Verschuere, S. Diamond, and S. Boyd, "A rewriting system for convex optimization problems," *Journal of Control and Decision*, vol. 5, no. 1, pp. 42–60, 2018.
- [31] M. Shahidehpour and Y. Fu, "Benders decomposition in restructured power systems."
- [32] G. Larroux, M. Jacobs, and M. Paolone, "On the tightness of the second-order cone relaxation of the optimal power flow with angles recovery in meshed networks," 2026, arXiv:2602.16866.
- [33] A. B. Birchfield, T. Xu, K. M. Gegner, K. S. Shetye, and T. J. Overbye, "Grid structural characteristics as validation criteria for synthetic networks," *IEEE Transactions on Power Systems*, vol. 32, no. 4, pp. 3258–3265, 2017.

## APPENDIX

### A. Convergence for mixed-integer master problem variables

Finite convergence of the GBD algorithm is established here for a master problem comprising both integer and continuous variables, with the continuous variables restricted to a convex set. In [26], finite convergence is guaranteed if either (i) the master-feasible set  $Y$  is finite, or (ii)  $Y$  is a compact (i.e., closed and bounded) subset of the feasible set of the linking variables in all subproblems, denoted by  $V$ . In brief, case (i) follows from the finiteness of  $Y$  and from the fact that the master problem cannot generate the same solution more than once. Case (ii) relies on the existence and uniform boundedness of the optimal dual multiplier vectors of the subproblems for all  $y \in Y$ , which is ensured if Slater's constraint qualification holds at each such point. Consequently, if all values of the linking variables that lead to infeasible subproblems are eliminated in finitely many iterations, and if the remaining master-feasible set is a compact subset of  $V$ , finite convergence follows.

For the problem considered in this work, subproblem infeasibility can only occur when the master sets the siting decision to zero at a candidate location, i.e., when a BESS is not installed. Since the number of such binary configurations is finite, all infeasible siting patterns can be excluded in finitely many iterations. After their exclusion, the remaining master-feasible region is a finite union of Cartesian products of

bounded continuous domains (2D boxes for sizing variables) with binary decisions. Hence, it is contained in a bounded hyper-rectangle and is therefore a compact subset of  $V$ . This implies finite convergence of GBD by Theorem 1 in [26].

### B. Feasibility check subproblem formulation

Consider the feasibility-check subproblem (FSBP) as formulated in [31] (see the reference for the notation). Note that this construction extends to conic constraints via the generalized Farkas lemma, as shown in [28].

$$\begin{aligned} & \min_{\mathbf{x} \geq \mathbf{0}} && \mathbf{1}^T \mathbf{s} \\ \text{(FSBP)} : & \text{s.t.} && \mathbf{E}\mathbf{x} + \mathbf{I}\mathbf{s} \geq \mathbf{h} - \mathbf{F}\mathbf{y} && : \mathbf{u} \\ & && \mathbf{y} = \hat{\mathbf{y}} && : \rho \\ & && \mathbf{s} \geq \mathbf{0} && : \lambda \end{aligned} \quad (14)$$

The authors argue that (FSBP)' is a particular instance of (FSBP), which yields the same feasibility cuts formulation.

$$\begin{aligned} & \min_{\mathbf{x} \geq \mathbf{0}} && \mathbf{1}^T \mathbf{s} \\ \text{(FSBP)}' : & \text{s.t.} && \mathbf{E}\mathbf{x} \geq \mathbf{h} - \mathbf{F}\mathbf{y} && : \mathbf{u}' \\ & && \mathbf{y} = \hat{\mathbf{y}} + \mathbf{s} && : \rho' \\ & && \mathbf{s} \geq \mathbf{0} && : \lambda \end{aligned} \quad (15)$$

Feasibility cuts follow from strong duality: for a minimization problem, the dual objective provides a lower bound on the primal optimum. Moreover, subproblem feasibility (equivalently, zero optimal slack) implies that the primal optimal value equals 0. Therefore, subproblem feasibility requires  $\inf_{\mathbf{x} \geq \mathbf{0}, \mathbf{y}, \mathbf{s}} \mathcal{L}(\mathbf{x}, \mathbf{y}, \mathbf{s}) \leq 0$ . The derivation of the left-hand side of this inequality constraint proceeds identically for both (FSBP) and (FSBP)', with the only difference being a linear transformation of the slack variables by  $\mathbf{F}$ . The latter is less general, as it enforces  $\dim(\mathbf{s}) = \dim(\mathbf{y})$  rather than matching the dimension of the constraint residuals; consequently, infeasibilities that cannot be resolved by relaxing only the linking variables cannot be represented in formulation (FSBP)'.

The Lagrangian function associated with (FSBP) is given by (16).

$$\begin{aligned} \mathcal{L}(\mathbf{x}, \mathbf{y}, \mathbf{s}) = & \mathbf{1}^T \mathbf{s} + \mathbf{u}^T (\mathbf{h} - \mathbf{F}\mathbf{y} - \mathbf{E}\mathbf{x} - \mathbf{I}\mathbf{s}) \\ & + \rho^T (\mathbf{y} - \hat{\mathbf{y}}) - \lambda^T \mathbf{s}, \end{aligned} \quad (16)$$

This yields the first-order optimality conditions (17) and complementarity slackness conditions (18).

$$\begin{aligned} \nabla_{\mathbf{x} \geq \mathbf{0}} \mathcal{L}(\mathbf{x}, \mathbf{y}, \mathbf{s}) &= -\mathbf{E}^T \mathbf{u} = 0 \\ \nabla_{\mathbf{y}} \mathcal{L}(\mathbf{x}, \mathbf{y}, \mathbf{s}) &= \rho - \mathbf{F}^T \mathbf{u} = 0 \\ \nabla_{\mathbf{s}} \mathcal{L}(\mathbf{x}, \mathbf{y}, \mathbf{s}) &= \mathbf{1} - \mathbf{I}\mathbf{u} - \lambda = 0, \\ \mathbf{h} - \mathbf{F}\mathbf{y} - \mathbf{E}\mathbf{x} - \mathbf{I}\mathbf{s} &= 0, \quad \mathbf{u} > 0 \\ \mathbf{s} > 0, & \quad \lambda = 0. \end{aligned} \quad (17)$$

The dual objective is then given by (19), which yields the feasibility cut  $\rho^T (\mathbf{y} - \hat{\mathbf{y}}) + v(\hat{\mathbf{y}}) \leq 0$ .

$$\begin{aligned} \inf_{\mathbf{x} \geq \mathbf{0}, \mathbf{y}, \mathbf{s}} \mathcal{L}(\mathbf{x}, \mathbf{y}, \mathbf{s}) &= \mathbf{u}^T \mathbf{h} - \rho^T \hat{\mathbf{y}} \\ &= \mathbf{u}^T (\mathbf{F}\mathbf{y} + \mathbf{E}\mathbf{x} + \mathbf{I}\mathbf{s}) - \mathbf{u}^T \mathbf{F}\hat{\mathbf{y}} \\ &= \mathbf{u}^T \mathbf{F} (\mathbf{y} - \hat{\mathbf{y}}) + (\mathbf{1} - \lambda)^T \mathbf{s} \\ &= \rho^T (\mathbf{y} - \hat{\mathbf{y}}) + \mathbf{1}^T \mathbf{s}. \end{aligned} \quad (19)$$